Ge quantum dots encapsulated by AlAs grown by molecular beam epitaxy on GaAs without extended defects

Meng Qi (齐蒙), Chad A. Stephenson, Vladimir Protasenko, William A. O'Brien, Alexander Mintairov, Huili (Grace) Xing, and Mark A. Wistey[a)]
Electrical Engineering, University of Notre Dame, Notre Dame, Indiana 46556, USA

(Received 6 November 2013; accepted 6 February 2014; published online 21 February 2014)

We demonstrate nearly spherical, strain-free, self-assembled Ge quantum dots (QDs) fully encapsulated by AlAs, grown on (100) GaAs by molecular beam epitaxy. The QDs were formed without a wetting layer using a high temperature, *in situ* anneal. Subsequent AlAs overgrowth was free from anti-phase domains and threading dislocations in cross section transmission electron microscopy. The straddling band alignment for Ge in AlAs promises strong and tunable confinement for both electrons and holes. The reflection high-energy electron diffraction pattern changed from 2×3 to 2×5 with anneal, which can be explained by surface reconstructions based on the electron-counting model. © *2014 AIP Publishing LLC*. [http://dx.doi.org/10.1063/1.4866278]

Germanium quantum dots (QDs) have interesting properties such as a large exciton binding energy, long radiative lifetime, and strong size dependence of radiative lifetime,[1] which could be utilized for optical devices. In particular, as an indirect bandgap material, Ge can offer long minority carrier lifetimes, ranging from μs to ms.[2,3] However, carrier confinement in Ge nanostructures is difficult without lattice matched energy barrier materials. Ge QDs, reported to date, have nearly all been grown on Si, with QD formation occurring by a Stranski-Krastanov (SK) growth mode driven by the 4% strain between Ge and Si.[4–6] However, Si barriers provide relatively weak confinement for holes and none for electrons. Furthermore, SK growth leaves a wetting layer that prevents subsequent III-V layers from being registered to the underlying substrate. This can lead to anti-phase domains (APDs) due to the growth of polar III-V's on non-polar Ge.[7–11] Ge nano-crystals in a dielectric matrix have been well studied and show different photoluminescence (PL) emission in the visible light range.[12–15] Such emission is attributed to excitonic emission in a quantum-confined system.[15–17] However, this technique shows poor interfaces between the dielectric and the Ge nano-crystals, which can influence the optical emission properties.[18,19] Emission in the near infrared has also been demonstrated,[20,21] and size-dependent emission has been theoretically calculated.[22]

Embedding Ge nanostructures in a wider bandgap material such as AlAs could offer advantages for up-conversion solar cells, light emitting devices, single electron tunneling devices, and other optoelectronics. Type-I (straddling) band alignment of the AlAs/Ge heterojunction and full encapsulation in all three dimensions would provide strong quantum confinement for both electrons and holes. Prevention of APDs normally requires special efforts.

In this work, self-assembled Ge QDs were formed directly on (100) AlAs by thin (0.55 or 1.1 monolayer (ML)) Ge deposition followed by *in situ* high temperature annealing. Ge and AlAs are nearly lattice-matched, so QD ripening is not primarily driven by strain. The resulting Ge QDs were nearly spherical, and the AlAs was free of any Ge wetting layer between the QDs.

The growths were carried out in several interconnected MBE chambers including a Veeco Gen 930 for III-V semiconductors and an Intevac Mod Gen II for Group IV semiconductors. The growth temperatures were calibrated by a kSA BandiT system, which simultaneously measures temperature by pyrometry, band edge optical absorption, and blackbody radiation curves. As_2 was provided by a Veeco Mark V valved cracker. The growth rates were 1 μm/h for GaAs and AlAs, and 600 nm/h for Ge. In this growth, semi-insulating (100) GaAs substrates were heated to 630 °C for 15 min to fully desorb surface oxides. Then 200 nm of non-intentionally doped GaAs and 200 nm AlAs were grown at 610 °C with a V/III beam equivalent pressure ratio of 20. The sample was then cooled to room temperature, with As flux maintained until below 400 °C to prevent decomposition. The sample was transferred under UHV to the Group IV chamber for solid source Ge growth. Either 0.55 or 1.1 ML of Ge was grown at 410 °C. The sample was then transferred back to the III-V chamber for annealing at 690 °C. A beam equivalent pressure of $As_2 = 6.7 \times 10^{-6}$ Torr was used to prevent decomposition of the AlAs above 400 °C during the anneal. After the anneal, several samples were overgrown with cap layers of AlAs and GaAs. To minimize oxidation, each sample was unloaded quickly and immediately placed in an N_2 purged glovebag. Uncapped samples were then loaded under inert gas into an Ar-purged atomic force microscope (AFM) to explore the surface morphology, as shown in Fig. 1. In addition, transmission electron microscopy (TEM) specimens were prepared by focused ion beam (FIB) to get uniform, 100 nm thick specimens. Cross-section high resolution TEM (HRTEM) and scanning TEM (STEM) results were used to characterize nano-scale geometry and structure, as shown in Fig. 2.

AFM of uncapped samples confirmed the formation of Ge QDs, as shown in Fig. 1. A control sample had 0.55 ML of Ge on AlAs without annealing and showed a smooth surface without QD formation. Deposition and annealing of 0.55 ML Ge formed QDs with a density of 6×10^9 cm^{-2} after 10 min at 690 °C, while 1.1 ML formed larger QDs with a

[a)]Electronic mail: mwistey@nd.edu. Tel.: (574) 631-1639. Fax: (574) 631-4393.

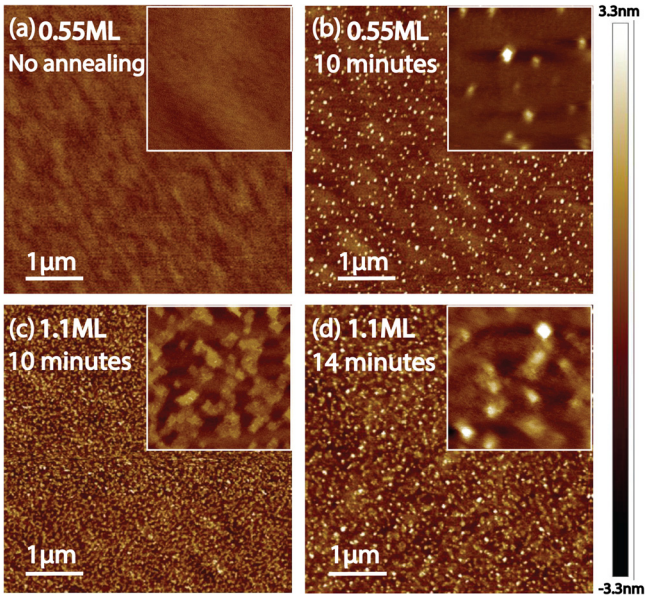

FIG. 1. AFM under inert gas of uncapped Ge QDs on AlAs, with 690 °C anneal. (a) 0.55 ML of Ge without annealing, (b) 0.55 ML Ge after 10 min anneal, (c) 1.1 ML Ge with 10 min anneal, (d) 1.1 ML Ge with 14 min anneal. Insets are higher magnification 500 nm by 500 nm scan.

density of $2.8 \times 10^{10}\,\mathrm{cm}^{-2}$. For the 1.1 ML initial Ge layer, a longer anneal of 14 min at the same temperature further increased the size and reduced the density of QDs to $5.6 \times 10^{9}\,\mathrm{cm}^{-2}$, consistent with Ostwald ripening,[23,24] which has demonstrated similar island formation on silicon.[25] This indicates the growth mechanism is surface energy driven.

The absence of a wetting layer provides ample exposed III-V surface for subsequent growth of additional AlAs without APDs. The RHEED during the III-V overgrowth to encapsulate the QDs showed the same bright and faint 2×4 patterns as normal GaAs and AlAs growth, respectively. HRTEM (Fig. 2) revealed the geometry of the QD structure.

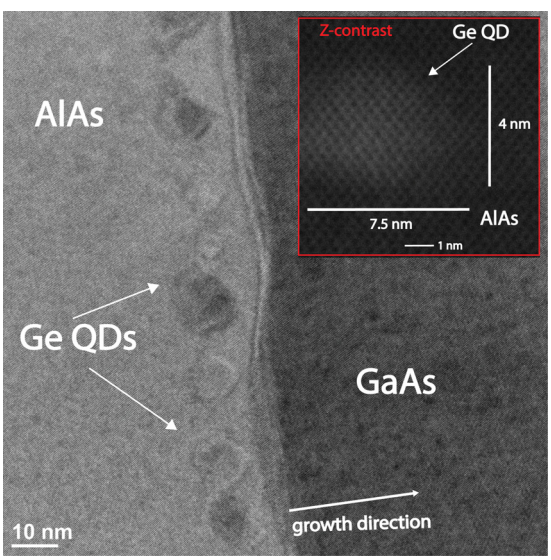

FIG. 2. Cross-section HRTEM shows QDs formed by annealing of 1.1 ML Ge on AlAs, followed by subsequent AlAs and GaAs overgrowth. The inset shows a Z-contrast STEM lattice image. Lattice of Ge QDs with higher contrast can be observed with AlAs lattice around. The dimensions of a single Ge QD are measured in the inset figure. Note lack of a wetting layer in STEM mode.

Ge QDs were fully encapsulated in AlAs, with AlAs and GaAs subsequent layers grown on top. No threading dislocations or APDs were visible in cross section TEM, indicating high quality overgrowth by AlAs and GaAs. The inset Z-contrast image in Fig. 2 shows a single Ge QD surrounded by AlAs. The contrast came from the average atomic mass difference between Al and Ge in this region. A continuous lattice structure for both the QD and the host AlAs can be observed, along with a QD lateral diameter of 7 nm and vertical height of 4.5 nm. The height from HRTEM is consistent with the height from AFM. The AFM shows a lateral diameter of 15–25 nm, which may be limited by the geometry of the AFM tip.

Raman spectroscopy was used to characterize the Ge content in the QDs. In Fig. 3, the inset shows the structure of the measured sample. A 1 μm $Al_{0.4}Ga_{0.6}As$ buffer followed by 1 μm AlAs was grown on GaAs in order to absorb the pump laser and thus prevent Raman peak from the GaAs substrate, since the Raman peak of bulk GaAs at 291.5 cm^{-1} is close enough to that of bulk Ge at 300.5 cm^{-1} that they might overlap. A 5 nm $Al_{0.4}Ga_{0.6}As$ cap layer on top of four periods of 1.1 ML Ge QDs/15 nm AlAs was used to prevent the rapid oxidation of AlAs. Raman spectroscopy showed a peak at 299 cm^{-1}, which we attribute to the LO phonon of Ge, 300.5 cm^{-1}, shifted about 1.5 cm^{-1}. The downshift of the Ge Raman peak was likely caused by sample heating from the Raman pump laser, based on power-dependent measurements (not shown).[26] Also, the line shape of the Ge QDs was observed to be asymmetric. Similar asymmetric line shapes have been reported for InAs/AlAs QDs and other arsenide material systems.[27] A similar asymmetric phonon line shape for Ge QDs is characteristic of Raman spectra of nanocrystalline structures, which can be described by a model of phonon confinement in nanoclusters of inhomogeneous size.[28,29] The clear Ge peak in Raman spectroscopy suggests that the Ge QDs are at least relatively pure.

The RHEED patterns before and after annealing at the same temperature as well as during annealing at 690 °C are shown in Fig. 4. The conventional 2×4 RHEED pattern for AlAs was not observed during the annealing. Before

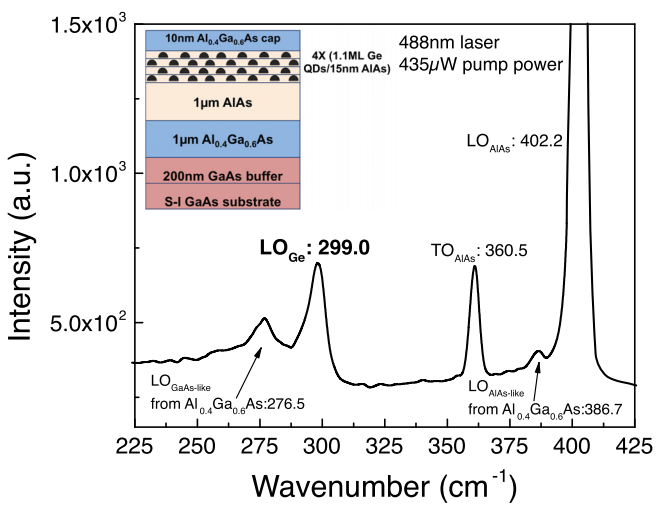

FIG. 3. Raman spectroscopy of Ge QDs. The LO phonon peak of Ge is observed at 299 cm^{-1}. Other peaks[40] from the $Al_{0.4}Ga_{0.6}As$ and AlAs buffer are also labeled. The sample structure is shown schematically in the inset.

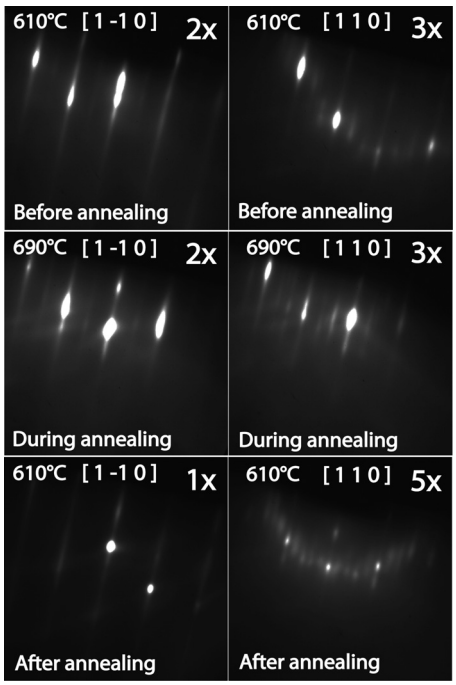

FIG. 4. RHEED patterns observed at substrate temperatures of 610 °C before annealing (top row), 690 °C during annealing (middle row), and 610 °C after annealing (bottom row). 0.55ML of Ge was deposited on AlAs before annealing. A 2×3 pattern was observed before and during annealing since there is one weak line between the main lines at [1 −1 0] and two weak lines between mainlines at [1 1 0]. Some of the samples show weak 2×5 after the annealing at 610 °C instead of 1×5 under the same condition. All the samples were grown on (0 0 1) GaAs substrates.

annealing, a clear streaky 2×3 RHEED reconstruction pattern was observed for the 0.55 ML Ge/AlAs surface at 610 °C, as shown in the upper figure in Fig. 4. During the annealing, the 2×3 pattern became more diffuse, and the streaky lines became less continuous, which was consistent with QD formation. After annealing, a unique 1×5 or weak 2×5 was observed. In order to correlate the RHEED pattern to the QD formation mechanism, a surface reconstruction model is proposed in Fig. 5, based on the electron-counting model.[30] At relatively low temperature before annealing, the initial Ge layer is uniformly distributed, confirmed by the streaky 2×3 RHEED pattern and AFM (Fig. 1(a)). Given the fact that Ge can sit on either Group III or Group V sites for GaAs and $Al_xGa_{1-x}As$, the overall conductivity depends on the relative availability of the two kinds of crystal vacancies under given growth conditions.[31–35] Since there was a high As flux during the annealing step to form Ge QDs, the surface is highly As-rich, confirmed by the reconstructions on bare GaAs and AlAs (not shown). The equilibrium is therefore pushed toward Ge on Group III sites. With a single Ge_{Al} substitution in the 2×3 unit cell shown in Fig. 5(a), the cell fulfills the electron-counting rule and becomes a stable surface reconstruction. Also, the 2×3 reconstruction arises from the one missing As-As dimer for every two dimers. Additional Ge_{Al} and Ge_{As} substitutions may allow other stable surface reconstructions based on electron-counting model, as shown in Fig. 5(c). During the annealing at around 700 °C, the Ge atoms become more mobile due to the higher kinetic energy, and we believe the surface reconstruction

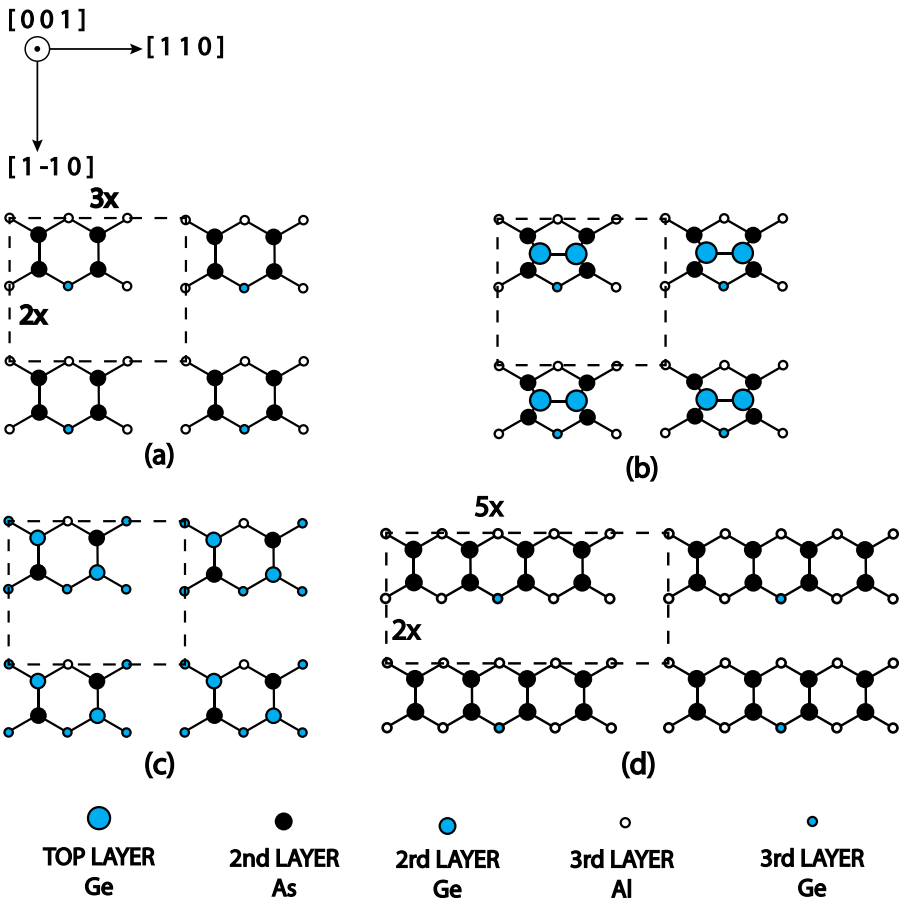

FIG. 5. Unit cells of surface reconstruction model based on electron counting model for 2×3 (a)–(c) and 2×5 (d) RHEED patterns. (a), (b) Show possible surface reconstructions before annealing in areas with <1 ML Ge. One Al atom is replaced by Ge atom in each unit to fulfill electron-counting rules. (b) Unit cell with a Ge-Ge dimer on top which gives a higher Ge concentration. (c) Possible surface reconstruction before annealing with higher Ge content before annealing with >1 ML Ge, five Al and two As atoms are replaced by Ge atoms in each unit cell. (d) Surface reconstruction of non-QD area after annealing with a much lower Ge concentration. Only one example of possible unit cell structures is shown for each configuration.

favors Ge-Ge bonds over Ge-As bonds. Fig. 5(b) shows a 2×3 unit cell with a Ge-Ge dimer on top still fulfilling the electron-counting model. Several possible stable 2×3 surface reconstructions with different Ge concentrations, as shown in Figs. 5(a)–5(c)), can show the 2×3 pattern that was observed for samples with different initial Ge thicknesses. The anneal changes the Ge distribution, and most of the surface has much less Ge coverage due to the QD formation. With one Al atom replaced by Ge, the 2×5 becomes a stable structure, as shown in Fig. 5(d). This is consistent with the reduced Ge coverage over most of the surface. The high temperature annealing also makes long range ordering feasible, thus allowing the 2×5 surface reconstruction as observed in RHEED. Further experiments will be performed to test this theory by altering the surface and formation energies of the QDs using various terminating species.

We believe the growth mechanism for self-assembly of Ge QDs on AlAs is driven by a high surface energy, caused by Ge atoms avoiding the As bonds at high temperature.[31] At lower temperatures such as during Ge deposition, Ge atoms have a low surface mobility, and As is similarly stable in its bonds with Al. This prevents atomic rearrangement but leads to an energetically unfavorable surface due to the violation of electron counting.[36] During annealing, however, Ge reduces its surface energy by forming Ge QDs with a high aspect ratio, removing most of the Ge from the surface. The lack of a wetting layer is due to the strain-free relaxation mechanism, since there is an energetic penalty for the first monolayer due to broken bonds, but no additional penalty for additional monolayers. The observation of Ostwald ripening as shown in Fig. 1 suggests that QDs are driven toward a lower surface-to-volume ratio with larger, more stable QDs. This indicates atoms on the QD surfaces are especially unfavorable due to dangling bonds, which are only partly relieved by reconstruction or bonded excess As.

Based on the Al-As-Ge alloy phase diagram, AlAs has a solubility limit less than 2% in Ge at around 700 °C, and a eutectic temperature at 735 °C.[37,38] Although there is a Al-Ge eutectic point at temperatures as low as 420–425 °C,[39] no change is visible in RHEED until near the annealing temperature of 690 °C during the MBE growth. To explain this, we suggest that Ge and Al have insufficient surface mobility at low temperature to gather into droplets, or else the presence of arsenic may suppress the Ge-Al eutectic formation. At annealing temperature, we believe the presence of the free surface reduces the eutectic temperature of Ge-AlAs, and the alloy becomes droplets as Al is dissolved from the AlAs layer. When the substrate is cooled under As_2, the alloy may segregate into AlAs and Ge, but it retains the circular shape and high aspect ratio of droplets. Better recrystallization conditions, such as cooling slowly through the freezing point under As rich conditions, may increase the crystal quality by favoring the growth of AlAs as it segregates from the melt.

In summary, we have demonstrated self-assembled Ge QDs grown on AlAs. The QDs completely consumed the Ge wetting layer, using a high temperature annealing step. The lack of a wetting layer allowed subsequent growth of additional AlAs without APDs to fully encapsulate the Ge QDs. Raman spectroscopy confirmed the high-purity Ge based on a peak at 299 cm^{-1}. The downshift of 1.5 cm^{-1} from the bulk Ge Raman peak for the Ge QD phonon is attributed to thermal heating during measurement. An asymmetric Raman line shape is likely caused by the inhomogeneous sizes of the QDs as well as possibly phonon confinement. Ostwald ripening was observed, which confirmed that the self-assembly growth mechanism of Ge QDs on AlAs originates from the surface free energy and surface tension of Ge on AlAs at the annealing condition. RHEED patterns of 2×3 and 2×5, uncommon in AlAs, were observed before and after the Ge QD formation, respectively. A surface reconstruction model based on the electron-counting rule was proposed and used to explain the observed reconstructions. This growth technique can offer an APD-free combination of Group IV and III-V materials, as well as direct and indirect bandgaps (if AlGaAs is used), for device applications.

The authors thank Dr. Xinyu Liu, James Kapaldo, Guowang Li, and Pei Zhao at University of Notre Dame for helpful discussions and the Notre Dame Integrated Imaging Facility (NDIIF).

[1]T. Takagahara and K. Takeda, Phys. Rev. B **46**, 15578 (1992).
[2]S. R. Lederhandler and L. J. Giacoletto, Proc. IRE **43**, 477 (1955).
[3]E. Yablonovitch, D. L. Allara, C. C. Chang, T. Gmitter, and T. B. Bright, Phys. Rev. Lett. **57**, 249 (1986).
[4]K. L. Wang, D. Cha, J. Liu, and C. Chen, Proc. IEEE **95**, 1866 (2007).
[5]F. M. Ross, J. Tersoff, and R. M. Tromp, Phys. Rev. Lett. **80**, 984–987 (1998).
[6]J-M. Baribeau, X. Wu, N. L. Rowell, and D. J. Lockwood, J. Phys.: Condens. Matter **18**, R139 (2006).
[7]J. H. Neave, P. K. Larsen, B. A. Joyce, J. P. Gowers, and J. F. van der Veen, J. Vac. Sci. Technol. B **1**, 668 (1983).
[8]S. Strite, D. Biswas, N. S. Kumar, M. Fradkin, and H. Morkoç, Appl. Phys. Lett. **56**, 244 (1990).
[9]R. M. Sieg, J. A. Carlin, J. J. Boeckl, S. A. Ringel, M. T. Currie, S. M. Ting, T. A. Langdo, G. Taraschi, E. A. Fitzgerald, and B. M. Keyes, Appl. Phys. Lett. **73**, 3111 (1998).
[10]H. Tanoto, S. F. Yoon, W. K. Loke, E. A. Fitzgerald, C. Dohrman, B. Narayanan, M. T. Doan, and C. H. Tung, J. Vac. Sci. Technol. B **24**, 152 (2006).
[11]S. M. Ting and E. A. Fitzgerald, J. Appl. Phys. **87**, 2618 (2000).
[12]S. K. Ray, S. Maikap, W. Banerjee, and S. Das, J. Phys. D: Appl. Phys. **46**, 153001 (2013).
[13]Y. Maeda, Phys. Rev. B **51**, 1658 (1995).
[14]Y. Maeda, N. Tsukamoto, Y. Yazawa, Y. Kanemitsu, and Y. Masumoto, Appl. Phys. Lett. **59**, 3168 (1991).
[15]N. Shirahata, D. Hirakawa, Y. Masuda, and Y. Sakka, Langmuir **29**, 7401 (2013).
[16]W. K. Choi, Y. W. Ho, S. P. Ng, and V. Ng, J. Appl. Phys. **89**, 2168 (2001).
[17]A. K. Dutta, Appl. Phys. Lett. **68**, 1189 (1996).
[18]M. Zacharias and P. M. Fauchet, Appl. Phys. Lett. **71**, 380 (1997).
[19]K. S. Min, K. V. Shcheglov, C. M. Yang, H. A. Atwater, M. L. Brongersma, and A. Polman, Appl. Phys. Lett. **68**, 2511 (1996).
[20]S. Takeoka, M. Fujii, S. Hayashi, and K. Yamamoto, Phys. Rev. B **58**, 7921 (1998).
[21]C. Bostedt, T. van Buuren, T. M. Willey, N. Franco, L. J. Terminello, C. Heske, and T. Moller, Appl. Phys. Lett. **84**, 4056 (2004).
[22]E. G. Barbagiovanni, D. J. Lockwood, P. J. Simpson, and L. V. Goncharova, J. Appl. Phys. **111**, 034307 (2012).
[23]P. W. Voorhees, J. Stat. Phys. **38**, 231 (1985).
[24]J. A. Marqusee and J. Ross, J. Chem. Phys. **80**, 536 (1984).
[25]N. C. Bartelt, W. Theis, and R. M. Tromp, Phys. Rev. B **54**, 11741 (1996).
[26]A. Lugstein, M. Mijić, T. Burchhart, C. Zeiner, R. Langegger, M. Schneider, U. Schmid, and E. Bertagnolli, Nanotechnology **24**, 065701 (2013).
[27]D. A. Tenne, A. K. Bakarov, A. I. Toropov, and D. R. T. Zahn, Physica E **13**, 199 (2002).
[28]I. H. Campbell and P. M. Fauchet, Solid State Commun. **58**, 739 (1986).
[29]H. Richter, Z. P. Wang, and L. Ley, Solid State Commun. **39**, 625 (1981).
[30]M. D. Pashley, Phys. Rev. B **40**, 10481 (1989).

[31]W. Schairer and W. Graman, J. Phys. Chem. Solids **30**, 2225 (1969).
[32]A. Y. Cho and I. Hayashi, J. Appl. Phys. **42**, 4422 (1971).
[33]P. Gladkov and K. Ždánský, J. Appl. Phys. **80**, 3004 (1996).
[34]G. Oelgart, R. Schwabe, H. Fieseler, and B. Jacobs, Semicond. Sci. Technol. **3**, 943 (1988).
[35]G. Oelgart, B. Lippold, R. Heilmann, H. Neumann, and B. Jacobs, Phys. Status Solidi A **115**, 257 (1989).
[36]H. Kroemer, J. Cryst. Growth **81**, 193 (1987).
[37]F. R. Schmid, *Ternary Alloys* (VCH, 1994), Vol. 9, p. 97.
[38]J. H. Bryden, Acta Crystallogr. **15**, 167 (1962).
[39]P. Franke and D. Neuschütz, "Binary Systems. Part 1. Elements and Binary Systems from Ag-Al to Au-Tl," *Thermodynamic Properties of Inorganic Materials of Landolt-Börnstein - Group IV Physical Chemistry* (Springer, Berlin Heidelberg, 2002), Vol. 19, p. 151.
[40]G. S. Solomon, D. Kirillov, H. C. Chui, and J. S. Harris, J. Vac. Sci. Technol. B **12**, 1078 (1994).